

MightyLev: An acoustic levitator for high-temperature containerless processing of medium- to high-density materials

Cite as: Rev. Sci. Instrum. 95, 103903 (2024); doi: 10.1063/5.0221899

Submitted: 4 June 2024 • Accepted: 19 September 2024 •

Published Online: 9 October 2024



View Online



Export Citation



CrossMark

James W. E. Drewitt,^{1,a)} Barnaby Emmens,¹ Zhe-Hui Kong,¹ Bruce W. Drinkwater,² and Adrian C. Barnes¹

AFFILIATIONS

¹ School of Physics, University of Bristol, H H Wills Physics Laboratory, Tyndall Avenue, Bristol BS8 1TL, United Kingdom

² Department of Mechanical Engineering, University of Bristol, Queen's Building, University Walk, Bristol BS8 1TR, United Kingdom

^{a)} Author to whom correspondence should be addressed: james.drewitt@bristol.ac.uk

ABSTRACT

“MightyLev,” a new multi-emitter ultrasonic acoustic levitation device capable of extremely stable levitation of materials of density up to at least 11.3 g cm^{-3} , is described. The exceptional stability of medium- to high-density samples levitated in MightyLev makes the device highly suitable for chemical and structural analysis using micro-focused spectroscopic and x-ray scattering techniques. In combination with mid-infrared laser heating, MightyLev is capable of levitating metallic and oxide materials during high-temperature cycling and melting above 1500 K. Instabilities in particle confinement during heating were investigated by directly visualizing the acoustic field using schlieren imaging. The results reveal jets of hot-air directed along the anti-nodes of the acoustic field. The reaction force on the sample from the jet, coupled with the restoring force of the acoustic trap, generates a parametric lateral oscillation of the sample. This result provides valuable insight for future optimization and wider application of acoustic levitation for high-temperature containerless material processing.

© 2024 Author(s). All article content, except where otherwise noted, is licensed under a Creative Commons Attribution-NonCommercial 4.0 International (CC BY-NC) license (<https://creativecommons.org/licenses/by-nc/4.0/>) <https://doi.org/10.1063/5.0221899>

I. INTRODUCTION

High-temperature levitation is a valuable technique for processing liquid metals and oxide materials. By removing the need for a container, levitation eliminates contamination, chemical reactions, and heterogeneous nucleation at the sample-container interface. This facilitates the deep supercooling of liquids several 100 s of Kelvin below their melting temperatures, enabling the fabrication of solid glasses and other metastable phases that cannot be formed using conventional furnace methods.¹ The absence of a container is advantageous for *in situ* spectroscopy or diffraction analysis of liquids, as it enables the accurate measurement of a stably confined sample with minimal contribution from the sample environment.^{2–5}

Established techniques for high-temperature containerless processing and analysis of liquid metals and oxides include aerodynamic

levitation (ADL),⁴ electromagnetic levitation (EML),⁶ and electrostatic levitation (ESL).⁷ In ADL, the sample is suspended by aerodynamic forces generated by a stream of gas flowing through a diverging conical nozzle. In EML, eddy currents are induced in a sample in response to a magnetic field produced by a radio frequency coil. These currents cause induction heating and generate a Lorentz force, which counteracts gravity. In ESL, levitation is achieved using the Coulomb force acting on charged samples within an electrostatic field between opposed electrodes, with the sample position regulated via high-speed visual feedback control. In both ESL and ADL techniques, the sample is normally heated and melted using infrared (IR) lasers.

EML and ESL have been employed extensively in both ground- and space-based measurements of liquid metals and alloys.^{3,6–13} Aerodynamic levitation has been most widely used for the ground-based synthesis and characterization of oxide liquids

and glasses.^{2,4,5,14–21} Although these levitation techniques are well established as effective methods for high-temperature synthesis and analysis of materials, they do have limitations; EML requires the sample to be an electrical conductor and the temperature is indirectly controlled using an external gas flow, and ESL requires an electrically charged sample within a vacuum chamber. This limits the materials that can be processed and the conditions that can be achieved using these methods. In ADL, the sample's proximity ($\lesssim 1$ mm) to the levitation nozzle can cause instabilities and brief contact, resulting in crystallization and a risk of contamination. In addition, the levitation gas is at room temperature as it enters the nozzle, which cools the lower portion of the sample, giving rise to large temperature gradients across the sample.

Mid-air levitation at acoustic standing-wave nodes has been used for many years²³ and is a potential alternative approach for containerless processing of a wide-variety of materials. However, realizing the full potential of acoustic levitation requires the ability to levitate medium density oxide materials ($\sim 3\text{--}6 \text{ g cm}^{-3}$) and high-density metals (up to $\sim 12\text{--}16 \text{ g cm}^{-3}$) at high-temperatures. Until recently, acoustic levitation of materials of medium density (a few g cm^{-3}) has required the use of single or opposed pairs of high-powered Langevin horns to generate high acoustic pressures. These systems rely on highly tuned transducers and cavities. During operation, these transducers heat up, causing a change in their resonant frequency and effective height of the cavity, resulting in a loss of the stringent cavity resonance condition required for stable levitation. Practically, this means it is difficult to heat a levitated sample without continuous monitoring and tuning of

the levitator.²⁴ Nonetheless, Langevin horn based acoustic levitation systems have been reported to heat samples within external furnace chambers up to $\sim 1573 \text{ K}$ on Earth^{25–27} and up to 1800 K in Earth orbit during the Space Shuttle STS-61A mission for samples of density up to 4.2 g cm^{-3} .²⁷ A system of three orthogonal single-axis acoustic levitators in combination with Xenon lamps has been reported to successfully trap and heat samples on Earth at temperatures exceeding 2000 K .²⁸ Aero-acoustic systems, using a gas jet for levitation and Langevin-horn type transducers for stabilization, have been shown to levitate materials with densities up to 6.5 g cm^{-3} at temperatures up to 3500 K using laser heating.^{29,30} Despite these successful attempts, high-temperature containerless processing using acoustic levitation remains far from routine. Overcoming the inherent difficulty in maintaining the strict resonance conditions of Langevin-horn type transducers is crucial for the optimization and wider adoption of this method.

Recent advances in acoustic levitation have employed single-axis, non-resonant devices with phased arrays of low-voltage ultrasonic transducers. The “TinyLev” acoustic levitation device consists of $72 \times 10 \text{ mm}$ diameter 40 kHz ultrasonic piezoelectric “parking sensor” transducers arranged in a focusing condition to produce stable confinement of a variety of liquid- and solid-state materials of moderate density up to $\sim 3 \text{ g cm}^{-3}$.³¹ As TinyLev does not rely on a cavity resonance, it is insensitive to small changes in temperature and is capable of translating levitated samples by continuous phase adjustments of one bank of transducers. Using a precisely engineered and tuned TinyLev device, Contreras and Marzo³² demonstrated sustained levitation of steel and liquid mercury, although

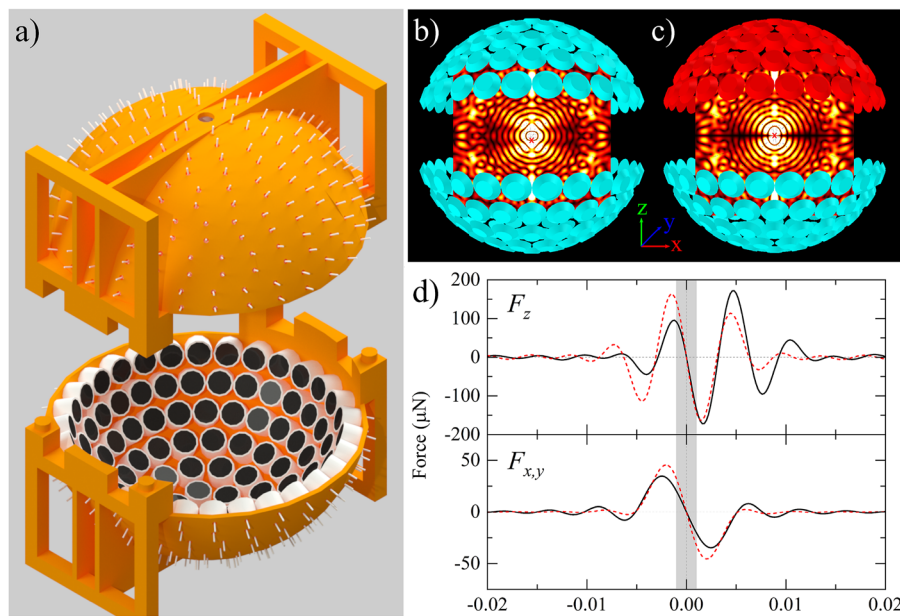


FIG. 1. (a) AutoCAD render of the MightyLev acoustic levitation device consisting of two arrays of $118 \times 16 \text{ mm}^2$ 40 kHz piezoelectric transducers mounted on 3D printed hemispheres of radius 9.5 cm . (b) The simulated acoustic pressure field for MightyLev with transducer arrays in-phase and (c) anti-phase for a peak-to-peak excitation voltage $V_{pp} = 15 \text{ V}$. (d) The longitudinal F_z and lateral $F_{x,y}$ forces, computed from the gradient of the Gor'kov potential²² for a 1.5 mm basalt glass sphere of density 2.90 g cm^{-3} placed at the acoustic nodes indicated by the red crosses in (b) (solid black curves) and (c) (red dashed curves).

the high excitation voltages required to levitate such high density samples impair their levitation stability. The “BigLev” device is a 160% scaled up version of TinyLev employing larger 16 mm diameter transducers for routine levitation of medium density samples up to 6.5 g cm^{-3} .³¹

In this paper, we describe the design and performance of “MightyLev,” a new non-resonant multi-transducer acoustic levitator with 16 mm transducers arranged in more closely spaced arrays compared to BigLev, with additional rows of transducers positioned toward the equatorial edges of the hemispherical arrays to enhance lateral stability. MightyLev is capable of highly stable levitation of medium- to high-density materials (up to at least 11.3 g cm^{-3}). In combination with CO₂ laser-heating, we demonstrate sustained levitation of materials in MightyLev at temperatures above 1500 K and examine heating induced instabilities using a schlieren imaging system.

II. Levitator Design and Performance

A. MightyLev design

MightyLev consists of two opposed 3D printed hemispheres of radius 9.5 cm on which 236×16 mm piezoelectric transducers (Manorshi, MSO-A1640H10T) are mounted [Fig. 1(a)]. Each transducer array is subdivided into quadrants, driven by separate L297N Dual H-Bridge motor drivers to amplify a 40 kHz square wave signal output from an Arduino Nano microcontroller. The Ultralino code³³ was used to predict the acoustic pressure field in MightyLev using Huygens’ principle and the acoustic forces using the Gor’kov model.²² The simulated acoustic pressure field for in-phase and anti-phase configurations of the transducer arrays is shown in Figs. 1(b) and 1(c), respectively. The calculated force experienced by a 1.5 mm diameter sphere of mid-ocean ridge basalt (MORB) glass, with density $\rho = 2.90 \text{ g cm}^{-3}$ and speed of sound $v = 6 \times 10^3 \text{ ms}^{-1}$,³⁴ placed at the central acoustic nodes for the in-phase and anti-phase configurations, is shown in Fig. 1(d) as a function of distance from the center of the particle. The ratio between the peak lateral force, F_{xy} , and the peak longitudinal force, F_z , is $\sim 1:3$, as compared to the $\sim 1:5$ ratio calculated for the same sample in the TinyLev and BigLev designs.³¹ This is due to the additional rows of transducers in MightyLev, positioned toward the equatorial edge of the hemispherical arrays and the closer separation of the arrays, which results in a more uniformly distributed trapping force in all directions and improves the lateral stability.

B. Stable levitation of medium- to high-density solids

The levitation capability of MightyLev was assessed by systematic levitation of millimeter-scale spheres of different densities in the central acoustic trap and determining the minimum peak-to-peak voltage (V_{pp}) required for levitation before the sample dropped. The minimum V_{pp} required for levitation of a range of solid samples is shown in Fig. 2 in comparison to the original TinyLev³¹ and optimized TinyLev variants.³² The response follows a linear trend within the experimental uncertainties. The slight deviations from linearity observed for samples of density $6\text{--}8 \text{ g cm}^{-3}$ can be attributed to small variations in sample diameter. Since the damping constant in an acoustic trap is proportional to mass, smaller mass samples are

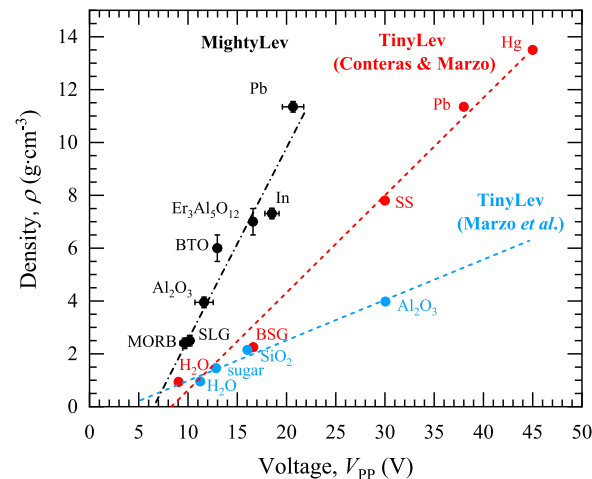


FIG. 2. Dropping voltage, i.e., the minimum excitation voltage required for levitation, for a range of spherical samples of diameter between 1 and 2 mm levitated in MightyLev (black; MORB = mid-ocean ridge basalt glass, SLG = soda-lime glass, Al₂O₃ = corundum, BTO = barium titanate glass, Er:Al₂O₃ = erbium aluminate glass, In = solid indium, and Pb = solid lead). For comparison, data are shown for TinyLev³¹ (blue; H₂O = water, sugar = sucrose crystal, SiO₂ = fused silica, and Al₂O₃ = sapphire) and an optimized TinyLev variant³² (red; H₂O = water, BSG = borosilicate glass, SS = stainless steel, Pb = solid lead, and Hg = liquid mercury).

less stable than larger mass samples of similar density at the same levitation voltage.

The minimum power consumption required to levitate a sample of the heavy metal Pb (density, $\rho \sim 11.3 \text{ g cm}^{-3}$) in MightyLev is $\sim 20 \text{ W}$ at $V_{pp} \sim 20 \text{ V}$. For routine stable levitation of Pb, a typical power consumption of $\sim 30\text{--}40 \text{ W}$ is required. This is comparable to the minimum power consumption of $\sim 40 \text{ W}$ required to levitate Pb in the TinyLev device at $V_{pp} \sim 38 \text{ V}$.^{31,32} However, while the three-dimensional stability of low-density samples (e.g., polystyrene and liquid water) levitated in TinyLev is good, the input voltages required to levitate high-density materials in TinyLev are close to or above the maximum recommended driving voltage of the piezoelectric transducers (typically $V_{RMS} \leq 30 \text{ V}$). Driving the transducers at high voltages causes heating of the piezoelectric ceramic and a shift in the resonance frequency. High-density samples levitated in TinyLev are visibly unstable, particularly with respect to lateral oscillations.³² In contrast, dense solids, including Pb, can be easily placed in the MightyLev trap for highly stable and sustained levitation at voltages well within the operational specifications of the transducers, with ample scope to increase the driving voltage if required to levitate higher-density materials or for heating experiments. As shown in video V1 of the [supplementary material](#), there is no significant visible movement of a range of medium- to high-density samples levitated in MightyLev.

Levitation stability can be quantified by the mean amplitude of oscillation and its standard error.³⁵ Mean displacements of $19(8) \mu\text{m}$ (longitudinal) and $189(30) \mu\text{m}$ (lateral) are observed for a 1.4 mm diameter Pb sphere after equilibration in the central trap of MightyLev. Smaller mean displacements of $7(4) \mu\text{m}$ (longitudinal) and $41(18) \mu\text{m}$ (lateral) are observed for a lower density 1.29 mm

diameter MORB sphere. The exceptional stability of medium- to high-density materials in MightyLev makes the device highly suitable for chemical and structural analysis using, e.g., micro-focused optical spectroscopy and x-ray scattering techniques.

To further quantify levitation stability and trap strength, high-frame rate (240 fps) digital videos were recorded for ~1.4 mm diameter MORB spheres levitated in (i) TinyLev, (ii) a variant of BigLev with reduced array separation, and (iii) MightyLev, during and after perturbation by a metal wire. Additional recordings were made for a larger (2.4 mm diameter) MORB sphere, a 1.4 mm diameter sphere of Pb, and a 3.2 mm diameter stainless steel ball bearing. The videos were recorded against a white background using a Panasonic Lumix GH5 II digital camera equipped with a Laowa 50 mm f/2.8 2X Ultra Macro lens. The image sequences were analyzed frame-by-frame to track the sample position using the connected components analysis function “regionprops” available in the MATLAB Image Processing Toolbox. The centroid of connected components, as computed within a region of interest of a binarized image of the sample, was used to determine the horizontal and vertical position of the sample at each time step.

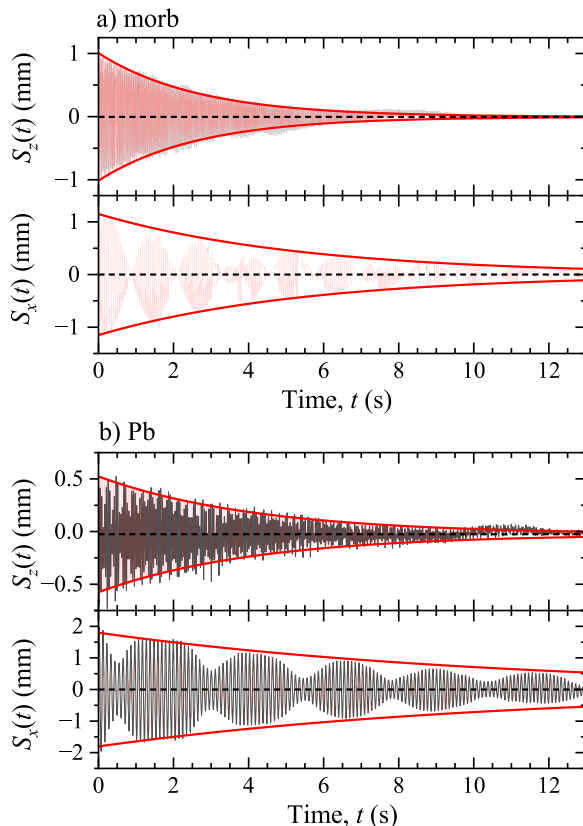


FIG. 3. Measured longitudinal and lateral displacements for the (a) MORB and (b) Pb samples levitated in MightyLev, as recorded after perturbation by a metal wire in 240 fps digital videos using the Lumix GH5 II camera (dark gray). The corresponding $S_z(t)$ and $S_x(t)$ functions modeled using Eqs. (1) and (2), respectively, are also shown (semi-transparent red) together with the exponential envelope (solid red curves).

Examples of the longitudinal and lateral displacement of MORB glass and Pb spheres in MightyLev after perturbation are shown in Fig. 3. The longitudinal displacement, $S_z(t)$, is effectively modeled by a damped cosine wavefunction of the form,

$$S_z(t) = S_{z,0} + A \exp\left(\frac{-t}{\tau}\right) \cos\left(\frac{\pi(t-\phi)}{T}\right), \quad (1)$$

where $S_{z,0}$ denotes the offset, t is the time, A is the amplitude at $t = 0$, τ is the exponential time constant, ϕ is the phase shift, and T is the oscillation period. For all designs of levitator (TinyLev, BigLev, and

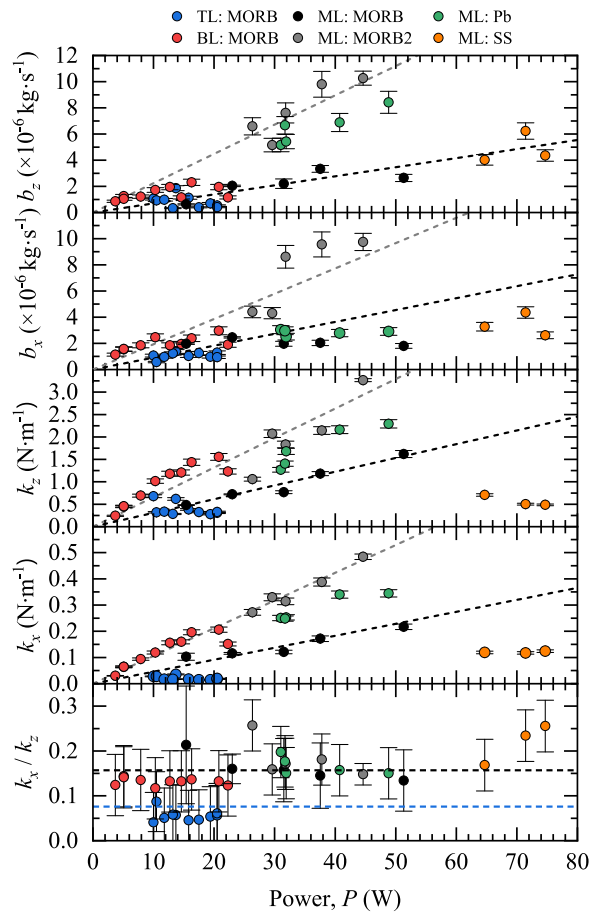


FIG. 4. Longitudinal (z) and lateral (x) damping b and spring k constants, shown as a function of power delivered to the transducers, for ~1.4 mm diameter spheres of MORB levitated in TinyLev (TL), a BigLev variant (BL), and MightyLev (ML). Data for a larger sphere of MORB (2.4 mm, MORB2), a Pb sphere (1.4 mm), and a 3.2 mm diameter stainless steel (SS) ball bearing, as levitated in MightyLev, are also shown. The black and gray dashed lines are fits to the data for the 1.4 and 2.4 mm diameter MORB spheres levitated in MightyLev, respectively. The bottom panel shows the ratio of lateral and longitudinal spring constants k_x/k_z , where the dashed black and blue lines are the ideal values from acoustic modeling of MightyLev and TinyLev designs, respectively, using the Ultraino code.³³

MightyLev), the lateral displacement, $S_x(t)$, exhibits a cosine amplitude modulation envelope of its underlying cosine waveform, which can be modeled by

$$S_x(t) = S_{x,0} + A \exp\left(\frac{-t}{\tau}\right) \cos\left(\frac{\pi(t - \phi)}{T}\right) \cos\left(\frac{\pi(t - \phi_{\text{mod}})}{T_{\text{mod}}}\right), \quad (2)$$

where ϕ_{mod} denotes the phase shift and T_{mod} denotes the period of the envelope modulation. By analogy to a mass-spring system, the acoustic trap can be considered as an under-damped linear harmonic oscillator system, with the oscillation period determined by the relation,

$$T = \frac{2\pi}{\sqrt{\frac{k}{m} - \left(\frac{b}{m}\right)^2}}, \quad (3)$$

where k denotes the spring constant, a measure of the trap stiffness, and m is the mass of the levitated sample. The damping constant, denoted b , is related to the time constant by

$$b = \frac{2m}{\tau}. \quad (4)$$

The longitudinal and lateral damping and spring constants were derived for the different levitator designs using Eqs. (3) and (4) are shown in Fig. 4 as a function of applied electrical power. In general, the damping and spring constants increase linearly with increasing power delivered to the transducers. The values obtained for a small ~ 1.4 mm diameter sphere of MORB glass levitated in MightyLev are comparable to those obtained from the BigLev variant. However, steeper gradients are observed in these values for the larger 2.4 mm diameter MORB sphere and the denser 1.4 mm diameter Pb sphere levitated in MightyLev. This is consistent with the direct proportionality of b to m and the dependence of k on both b and m . However, the values obtained for a 3.2 mm diameter stainless steel ball bearing levitated in MightyLev deviate from this trend, indicating the system may be operating at its performance limit or as a result of the Gor'kov criterion, which requires $r \ll \lambda$, where r is the object radius and $\lambda = 8.65$ mm is the wavelength of 40 kHz sound waves in the air. For the 3.2 mm ball bearing, the Gor'kov criterion is not strictly satisfied. The ratio of the lateral and longitudinal

spring constants k_x/k_z in TinyLev and MightyLev are consistent, within experimental uncertainties, with the theoretical values 0.076 and 0.157, respectively, computed from the acoustic field simulated in Ultraino³³ with no strong dependence on transducer power (Fig. 4).

III. CO₂ LASER HEATING SYSTEM

A class-I laser installation was constructed consisting of two class-IV 60 W mid-IR CO₂ lasers (Synrad Firestar Ti60) mounted on a 2×1 m² solid vibration isolation optical table (GZT-MOT-F20-10, Photonic Solutions) on two sides of an interlocked enclosure (Fig. 5). The enclosure was constructed from 2×2 cm² aluminum profile and 2 mm thick blackened steel sheets, with three access hatches (two front, one rear) secured individually by tongue operated fail-safe interlock switches (Trojan 5, Allen Bradley). The laser beams, with a fixed beam height of 32 cm from the base of the optical table, are incident into the interlocked enclosure at an angle of 15° from the horizontal axis via aluminum beam tubes and brought to convergence at a common focal point at the center point of the enclosure using 100 mm focal length plano-convex ZnSe lenses (Edmund Optics). IR absorptive graphite beam blocks (Thorlabs LB2/M, 1–12 μm, 80 W Max Avg. Power) are installed inside the enclosure to ensure the direct beam cannot impinge on the walls. During operation, a “Laser On” annunciator illuminates if the interlock condition is satisfied and one or both lasers are in operation. The enclosure is fitted with a feedthrough panel equipped with mains power, DC, USB-3, BNC, and Cat5e Ethernet sockets. MightyLev is mounted on a Gembitsu 1810 CNC router stage, modified for full three-axis translation, with motion controlled externally using a GRBL stepper motor control module. The levitated sample is monitored during heating using two Raspberry Pi HQ camera modules, equipped with Sony IMX477 12.3 Megapixel (4056×3040 pixels) image sensors and 16 mm telephoto C-mount lenses, each connected to individual 4 GB Raspberry Pi 4 (RPi-4) single board computers within the enclosure. The internal RPi-4 machines are linked to an external RPi-4 server via a gigabit Ethernet switch (D-Link, DGS-105). Data are shared and stored on the server using a network file sharing (NFS) protocol, with real-time images displayed using VNC remote access software. High frame rate (up to 240 fps) digital videos of



FIG. 5. (a) Schematic of the laser heating installation with dimensions indicated in cm. (b) Photograph of the completed construction. Two 60 W CO₂ Synrad Firestar Ti60 lasers are mounted on an optical table, each set at an angle of 15° from the horizontal axis with a fixed beam height of 32 cm. The laser beams are incident via beam tubes into an interlocked enclosure, constructed from a 2×2 cm² aluminum profile and 2 mm thick steel sheets. (c) Photograph of the interior of the laser enclosure with MightyLev installed.

the laser-heated levitated materials are recorded using the Panasonic Lumix camera operated remotely via a USB-tether.

A. Laser heating of levitated samples

Images from the low power laser heating tests of a 1.5 mm polystyrene sphere and gallium sample are shown in Fig. 6 (see also videos V2 and V3 of the [supplementary material](#), respectively). For the polystyrene sample [Fig. 6(a)], each laser was operated at 2.5 W, totaling 5 W. An indentation caused by the incident laser beam is visible on the sample after 4.2 ms. At ~60 ms, the sample undergoes expansion prior to melting at ~120 ms (melting point ~513 K), resulting in the eventual formation of a solid transparent disk of 1 mm diameter and 100 μm in thickness. For the gallium sample [Fig. 6(b)], due to its near room temperature melting point, single-sided laser heating was employed only with a maximum power of ~4 W. As the sample underwent melting, it elongated laterally within the acoustic trap, yet remained stably levitated with a slow rotation. On further heating, the molten gallium underwent further lateral

elongation before fragmenting into two distinct parts, which were expelled from the levitator.

The results of higher power laser heating tests, conducted using a MORB glass sample, are shown in Fig. 7. The lasers were operated at 6 W each, for a total of 12 W. Figure 7(a) shows a MORB sample during controlled heating, maintaining stable levitation throughout the process. After ~0.5 s of heating, the sample began to glow, reaching maximum luminosity ~1 s later, after which the sample was quenched while remaining levitated (see video V4 of the [supplementary material](#)). The results of a subsequent heating experiment are shown in Fig. 7(b). Here, the sample was laser heated for a more extended period, resulting in more pronounced luminosity. A pyrometer reading indicated a temperature surpassing 1200 K, although the significant instability of the sample precluded a precise temperature measurement. After ~5 s of heating, the sample appeared elongated laterally, indicating a molten sample, suggesting a temperature about 1500 K from the known melting point of MORB. During heating, lateral and longitudinal heating instabilities intensified, and after ~10 s of continuous heating, the sample was ejected from the trap (see video V5 of the [supplementary material](#)).

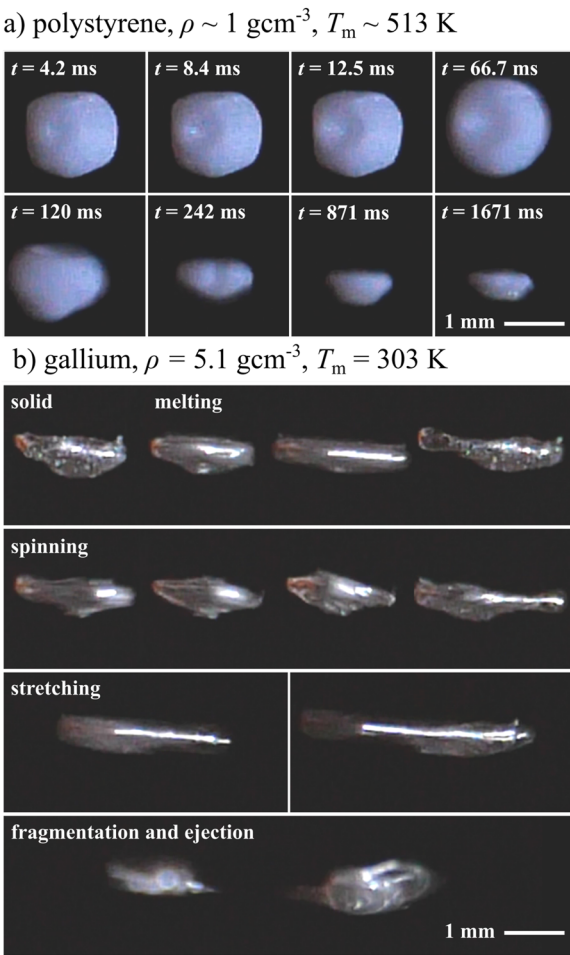


FIG. 6. Low temperature heating of (a) polystyrene and (b) gallium. Sample densities ρ and melting temperatures T_m are indicated in the captions.

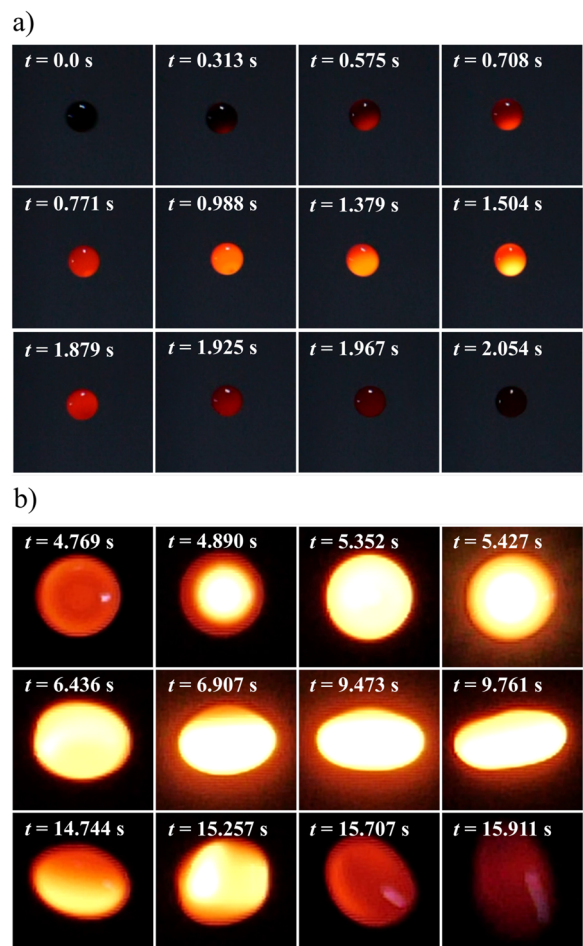


FIG. 7. High temperature heating of a MORB sample.

The heating tests reveal significant lateral oscillations induced in levitated samples during heating, even at low laser power. These oscillations increase with both laser power and duration. When levitation fails during heating, samples are typically ejected laterally across the traps rather than vertically. While MightyLev's enhanced lateral stability helps to mitigate this effect, understanding the origin of the induced lateral oscillations during heating is crucial for the future optimization of high-temperature mid-air acoustic levitation.

B. Schlieren imaging analysis

To investigate the cause of the instabilities that manifest during heating, a single-mirror on-axis schlieren³⁶ apparatus was constructed to image the acoustic field. The system, illustrated in Fig. 8, consisted of a spherical mirror (Luftvis Science, model D200F1280) of diameter $\phi = 0.2032(20)$ m and focal length $f = 1.28$ m (focal ratio $f/6.4$) held in a three-point adjustable mount. A bright (107 lm) white LED (Osram Duris E2835) light source was placed behind the two A2 tool steel blades of an adjustable mechanical slit (Thorlabs, VA100), with separation 2.8(1) mm, situated at a distance of $2f = 2.56(1)$ m along the optical axis of the mirror. The light from the LED source illuminates the mirror through the test region and is back reflected along the optical axis. A 25 mm visible wavelength non-polarizing beam splitter cube (Edmund Optics, A47-009) positioned in front of the light source diverts the reflected light to the imaging camera. The beam splitter was enclosed in a black fabric lined 3D printed case to prevent light external to the imaging axis from entering the optical system. To produce the schlieren effect, a 0.5 mm knife-edge was mounted on a high-precision manual 360° rotation stage and placed at the reflected image point. Light deflected by refractive index gradients in the test region, caused by, e.g., local variations in air density within an acoustic pressure field, can bypass the knife-edge filter, resulting in a schlieren image. Variations in the brightness of the image can thus be used to infer pressure gradients and the structure of the acoustic field.

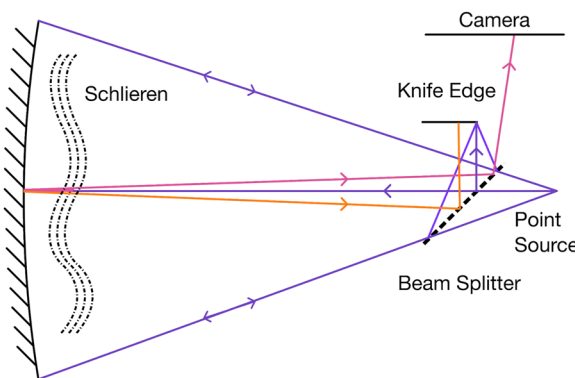


FIG. 8. Layout of the apparatus used to create schlieren images. A bright point light source illuminates the schlieren (i.e., acoustic field), and a large mirror focuses the light onto a knife edge. The purple lines show the path of light rays that are not deflected by the schlieren. The only rays that reach the camera are the ones that are deflected away from the knife edge, i.e., the pink line. The orange line shows the path of a ray with the opposite deflection angle.

The apparatus was tested first using a TinyLev device and IR lamp (Osram, HLX64635) focused on a levitated 1 mm diameter blackened sphere of polystyrene. The TinyLev device was oriented horizontally to direct heat from the transducers out of the device, preventing it from obscuring the image of the acoustic field. The knife edge was oriented vertically to determine the pressure gradients along the axis of the levitator. During heating, the sample is observed to oscillate vertically in its trap. The schlieren image, shown in Fig. 9 (see also video V6 of the [supplementary material](#)), reveals a jet of lower density air propagating away from the heated sample and directed along the longitudinal anti-nodes of the acoustic field. This discovery provides a possible explanation for the instabilities observed during laser heating: the interaction between the sample's reaction to the force of the jet, propagating along the anti-nodes of the acoustic field, and the restoring force of the field generates a parametric oscillation in the direction of acoustic pressure.

To verify this hypothesis, it was necessary to collect schlieren imagery during laser heating. However, due to MightyLev's size, the position of the mirror, and the need to operate CO₂ lasers in an interlocked enclosure, integrating MightyLev with the schlieren imaging system was not feasible. Instead, a 500 mW red-orange (638 nm) adjustable focus laser (OdicForce, DM-R500) was employed to heat a sample levitated in a TinyLev device, oriented vertically to replicate the geometry employed for laser-heating. A safety box enclosure (Euro Stacker, 600 × 400 × 400 mm³) was placed over the mirror to control reflections and cover the open beam path of the class 3B laser. The laser was incident on the sample, and fast frame rate (240 fps) schlieren images were recorded through an aperture cut into the box enclosure using the Panasonic Lumix GH5 II digital camera. As for the IR lamp test, a jet of hot, lower-density air was observed propagating from the sample along the anti-nodes of the field, producing concomitant lateral oscillations of the sample.

Due to the vertical orientation of the levitator, heat from the transducers impaired the schlieren image quality. To compensate for this, the knife-edge was set horizontally and adjusted to enhance the contrast of the acoustic field. This adjustment resulted in cropping of the schlieren image, producing a circular shadow on the mirror and aberrations around the image of the levitation device. Despite this,

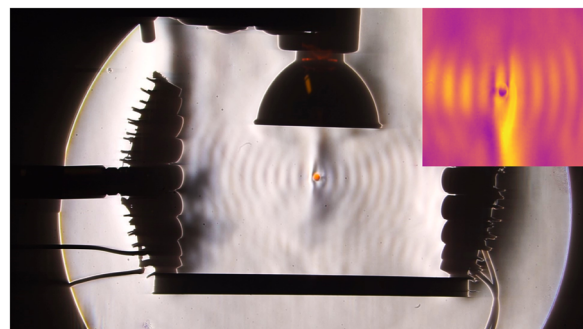


FIG. 9. Schlieren image of a heat lamp focused on a levitated polystyrene sphere in a TinyLev device. A focused jet of hot air is ejected from the trapping node, exerting a reaction force on the trapped object. The inset shows an image of the central region of the acoustic field with post-processing to remove optical defects and enhance contrast.

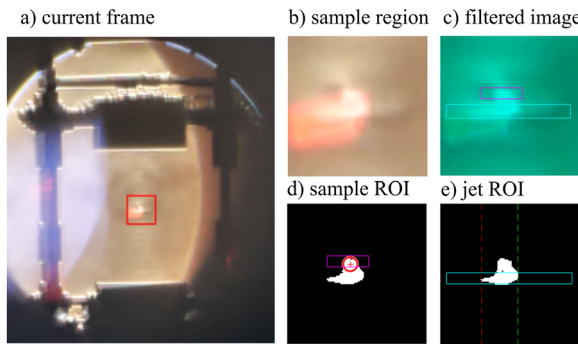


FIG. 10. (a) A frame taken from the schlieren video of a sample of polystyrene levitated in a TinyLev device and heated using a 500 mW 638 nm laser beam. (b) The isolated sample region corresponding to the red box in (a). (c) The image with an RGB mask applied to remove the red laser reflection. (d) The sample region of interest (ROI) (magenta rectangle), the sample (red circle), and centroid position (red cross). (e) The jet region of interest (green rectangle) and lateral extents (red and green dashed lines).

the image quality and visibility of refractive index gradients were sufficiently good for quantitative measurements of the sample and jet displacements to be made.

The schlieren image sequences during laser heating were analyzed frame-by-frame using the method illustrated in Fig. 10. The full analysis sequence is provided in video V7 of the [supplementary material](#). The sample region was isolated and an RGB mask applied to eliminate the red reflection from the incident laser. The subsequent image was binarized and the sample centroid position and maximum and minimum extents of the jet in the lateral direction

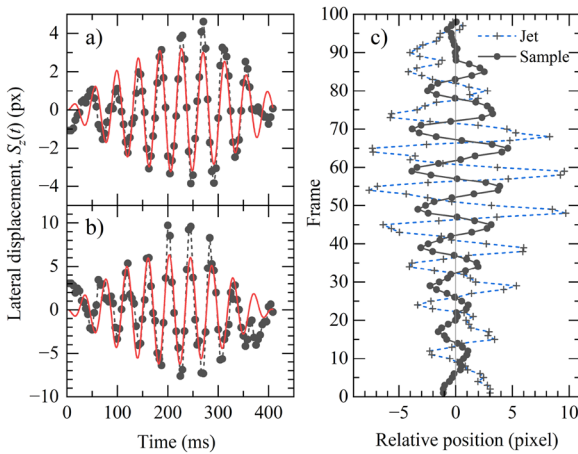


FIG. 11. (a) The lateral displacement of the sample and (b) the maximal extent of the jet for each frame of the schlieren video. A modulated sinusoidal waveform described by Eq. (5) is fit (red curves) to the displacement data (solid circles and dashed curves), with the parameters $S_{z,0} = -1.29 \times 10^{-2}$ px, $t_0 = 44.83$ ms, $T = 2.145 \times 10^{-2}$ ms, $A = 3.226$ px, and $T_2 = 441$ ms for the sample and $S_{z,0} = 6.6 \times 10^{-3}$ px, $t_0 = 23.96$ ms, $T = 0.021$ ms, $A = 6.330$ px, and $T_2 = 409$ ms for the jet. (c) Relative position of the sample center [solid (black circles and curve) and the maximum extent of the heating induced gas jet (plus sign and dashed blue curves)]

were determined. The lateral displacements $S_z(t)$ of both the sample and jet are shown in Figs. 11(a) and 11(b), respectively. The lateral displacements are effectively modeled using a modulated sinusoidal waveform function of the form,

$$S_z(t) = S_{z,0} + A \sin(\pi(t - \phi)/T) \sin(\pi t/T_2), \quad (5)$$

where $S_{z,0}$ is the zero offset, A is the amplitude, t is the time, ϕ is the phase shift, T is the period of oscillation, and T_2 is the period of sinusoidal modulation. In Fig. 11(c), the relative position of the sample and the maximum extent of the jet are plotted, revealing a striking anticorrelation between the two, i.e., the lateral displacement of the sample is driven in the opposite direction of the jet of hot air propagating from it. This reaction force, coupled with the restoring force of the acoustic trap, generates a parametric oscillation, which is the origin of the lateral instabilities observed during laser heating.

We attempted to mitigate this effect by heating the sample with a laser incident vertically from above. However, lateral instability remained. Consequently, we suggest that dynamic control mechanisms will be necessary to stabilize acoustic levitation during laser heating sufficiently to enable the application of *in situ* analysis of levitated samples at high-temperatures. Potential strategies include dynamic modulation of the acoustic field or pulse modulation of the heating laser to counteract the parametric oscillation.

IV. CONCLUSION

“MightyLev” is a new multi-emitter ultrasonic acoustic levitator capable of extremely stable levitation of medium- to high-density materials up to at least 11.3 g cm^{-3} . The extremely small (micro-scale) displacements observed during levitation make the device ideally suited for integration with micro-focused optical spectroscopy or x-ray scattering techniques for chemical and structural analysis. MightyLev’s capability to process high-density materials presents opportunities for the safe, contact-free handling and analysis of hazardous heavy-metal materials, such as uranium-containing molten salt coolants for next-generation fission reactors or intermediate-level nuclear waste.

In combination with mid-IR laser heating, we demonstrate stable levitation and melting of a synthetic polymer above 513 K, melting of the liquid metal gallium, and high-temperature cycling and melting of an oxide glass above 1500 K. Instabilities in particle confinement were investigated using schlieren imaging, revealing that parametric oscillations of the sample during heating are driven by hot jets of air propagating from the sample, coupled with the restoring force of the acoustic trap. This provides valuable insight for future optimization of the technique to enable the wider adoption of mid-air acoustic levitation for the synthesis and characterization of novel oxide and metallic glasses using *in situ* analysis at high-temperatures.

SUPPLEMENTARY MATERIALS

Videos V1–V7 referenced in the main text are provided as the [supplementary material](#). Video captions are provided below.

V1: Video demonstrating sustained acoustic levitation of medium- to high-density solids in MightyLev with exceptional stability. V2: Slow motion (240 fps) video showing melting of levitated

polystyrene using 5 W of mid-IR laser power. V3: Slow motion (240 fps) video showing melting of levitated gallium using 4 W of mid-IR laser power. V4: Slow motion (240 fps) video showing sustained levitation of a levitated MORB glass sample during laser heating and quenching. V5: Slow motion (240 fps) video showing melting of levitated MORB using 12 W of mid-IR laser power. V6: Schlieren imaging of a heat lamp focused on a levitated polystyrene sample in a TinyLev device, revealing a focused jet of hot air ejected from the trapping node. V7: Schlieren imaging (240 fps) analysis of the sample position and lateral extents of the jet during heating of a levitated polystyrene sphere using a 500 mW 638 nm laser.

ACKNOWLEDGMENTS

We gratefully acknowledge Tom Kennedy, Patrick Alexander, Adrian Crimp, and Joe Nunn for technical assistance. We thank Asier Marzo for helpful discussions and construction of the BigLev variant device. This research was funded by EPSRC standard Grant No. EP/V001736/1.

AUTHOR DECLARATIONS

Conflict of Interest

The authors have no conflicts to disclose.

Author Contributions

James W. E. Drewitt: Conceptualization (lead); Formal analysis (lead); Funding acquisition (equal); Investigation (lead); Methodology (lead); Software (lead); Writing – original draft (lead); Writing – review & editing (lead). **Barnaby Emmens:** Investigation (supporting); Methodology (supporting); Writing – review & editing (supporting). **Zhe-Hui Kong:** Investigation (supporting); Methodology (supporting); Writing – review & editing (supporting). **Bruce W. Drinkwater:** Conceptualization (supporting); Funding acquisition (supporting); Methodology (supporting); Writing – review & editing (supporting). **Adrian C. Barnes:** Conceptualization (supporting); Funding acquisition (equal); Methodology (supporting); Writing – review & editing (supporting).

DATA AVAILABILITY

Data are available at the University of Bristol data repository, data.bris.ac.uk, at <https://doi.org/10.5523/bris.6hu7y9f09t12l1goe5ln0vhz>.

REFERENCES

- ¹J. K. R. Weber, "The containerless synthesis of glass," *Int. J. Appl. Glass Sci.* **1**, 248–256 (2010).
- ²D. L. Price, *High-temperature Levitated Materials* (Cambridge University Press, 2010).
- ³I. Egry and D. Holland-Moritz, "Levitation methods for structural and dynamical studies of liquids at high temperatures," *Eur. Phys. J. Special Topics* **196**, 131–150 (2011).
- ⁴L. Hennet, V. Cristiglio, J. Kozaily, I. Pozdnyakova, H. E. Fischer, A. Bychkov, J. W. E. Drewitt, M. Leydier, D. Thiaudiére, S. Gruner, S. Brassamin, D. Zanghi, G. J. Cuello, M. Koza, S. Magazù, G. N. Greaves, and D. L. Price, "Aerodynamic levitation and laser heating: Applications at synchrotron and neutron sources," *Eur. Phys. J. Special Topics* **196**, 151–165 (2011).
- ⁵C. J. Benmore and J. K. R. Weber, "Aerodynamic levitation, supercooled liquids and glass formation," *Adv. Phys.: X* **2**, 717–736 (2017).
- ⁶D. Holland-Moritz, T. Schenk, P. Convert, T. Hansen, and D. M. Herlach, "Electromagnetic levitation apparatus for diffraction investigations on the short-range order of undercooled metallic melts," *Meas. Sci. Technol.* **16**, 372–380 (2005).
- ⁷P.-F. Paradis, T. Ishikawa, G.-W. Lee, D. Holland-Moritz, J. Brillo, W.-K. Rhim, and J. T. Okada, "Materials properties measurements and particle beam interactions studies using electrostatic levitation," *Mater. Sci. Eng. R* **76**, 1–53 (2014).
- ⁸I. Egry, G. Lohöfer, and G. Jacobs, "Surface tension of liquid metals: Results from measurements on ground and in space," *Phys. Rev. Lett.* **75**, 4043–4046 (1995).
- ⁹I. Egry, G. Lohöfer, E. Gorges, and G. Jacobs, "Structure and properties of undercooled liquid metals," *J. Phys.: Condens. Matter* **8**, 9363 (1996).
- ¹⁰D. Holland-Moritz, S. Stüber, H. Hartmann, T. Unruh, T. Hansen, and A. Meyer, "Structure and dynamics of liquid Ni₃₆Zr₆₄ studied by neutron scattering," *Phys. Rev. B* **79**, 064204 (2009).
- ¹¹T. Kordel, D. Holland-Moritz, F. Yang, J. Peters, T. Unruh, T. Hansen, and A. Meyer, "Neutron scattering experiments on liquid droplets using electrostatic levitation," *Phys. Rev. B* **83**, 104205 (2011).
- ¹²H. Tamaru, C. Koyama, H. Saruwatari, Y. Nakamura, T. Ishikawa, and T. Takada, "Status of the electrostatic levitation furnace (ELF) in the ISS-KIBO," *Microgravity Sci. Technol.* **30**, 643–651 (2018).
- ¹³M. Mohr, Y. Dong, G. P. Bracker, R. W. Hyers, D. M. Matson, R. Zboray, R. Frison, A. Dommann, A. Neels, X. Xiao, J. Brillo, R. Busch, R. Novakovic, P. Srirangam, and H.-J. Fecht, "Electromagnetic levitation containerless processing of metallic materials in microgravity: Thermophysical properties," *npj Microgravity* **9**, 34 (2023).
- ¹⁴S. Krishnan, J. J. Felten, J. E. Rix, J. K. R. Weber, P. C. Nordine, M. A. Beno, S. Ansell, and D. L. Price, "Levitation apparatus for structural studies of high temperature liquids using synchrotron radiation," *Rev. Sci. Instrum.* **68**, 3512–3518 (1997).
- ¹⁵A. C. Barnes, K. R. Whittle, and J. E. Enderby, "A determination of the electronic conductivity of aerodynamically levitated high temperature liquid metals and semiconductors by contactless methods," *J. Non-Cryst. Solids* **312–314**, 299–304 (2002).
- ¹⁶L. B. Skinner, A. C. Barnes, and W. Crichton, "Novel behaviour and structure of new glasses of the type Ba-Al-O and Ba-Al-Ti-O produced by aerodynamic levitation and laser heating," *J. Phys.: Condens. Matter* **18**, L407 (2006).
- ¹⁷J. W. E. Drewitt, S. Jahn, V. Cristiglio, A. Bychkov, M. Leydier, S. Brassamin, H. E. Fischer, and L. Hennet, "The structure of liquid calcium aluminates as investigated using neutron and high energy x-ray diffraction in combination with molecular dynamics simulation methods," *J. Phys.: Condens. Matter* **23**, 155101 (2011).
- ¹⁸J. W. E. Drewitt, L. Hennet, A. Zeidler, S. Jahn, P. S. Salmon, D. R. Neuville, and H. E. Fischer, "Structural transformations on vitrification in the fragile glass-forming system CaAl₂O₄," *Phys. Rev. Lett.* **109**, 235501 (2012).
- ¹⁹J. W. E. Drewitt, A. C. Barnes, S. Jahn, S. C. Kohn, M. J. Walter, A. N. Novikov, D. R. Neuville, H. E. Fischer, and L. Hennet, "Structure of liquid tricalcium aluminate," *Phys. Rev. B* **95**, 064203 (2017).
- ²⁰O. L. G. Alderman, L. Lazareva, M. C. Wilding, C. J. Benmore, S. M. Heald, C. E. Johnson, J. A. Johnson, H.-Y. Hah, S. Sendelbach, A. Tamalonis, L. B. Skinner, J. B. Parise, and J. K. R. Weber, "Local structural variation with oxygen fugacity in Fe₂SiO₄₊-fayalitic iron silicate melts," *Geochim. Cosmochim. Acta* **203**, 15–36 (2017).
- ²¹J. W. E. Drewitt, A. C. Barnes, S. Jahn, R. A. Brooker, L. Hennet, D. R. Neuville, and H. E. Fischer, "Iron coordination in liquid FeAl₂O₄," *Philos. Trans. R. Soc., A* **381**, 20220351 (2023).
- ²²L. P. Gor'kov, "Forces acting on a small particle in an acoustic field within an ideal fluid," *Dokl. Akad. Nauk SSSR* **140**, 88–91 (1961), see <https://www.mathnet.ru/eng/dan/v140/i1/p88>.

- ²³M. A. B. Andrade, N. Pérez, and J. C. Adamowski, "Review of progress in acoustic levitation," *Braz. J. Phys.* **48**, 190–213 (2018).
- ²⁴J. K. R. Weber, C. A. Rey, J. Neufeind, and C. J. Benmore, "Acoustic levitator for structure measurements on low temperature liquid droplets," *Rev. Sci. Instrum.* **80**, 083904 (2009).
- ²⁵R. R. Whymark, "Acoustic field positioning for containerless processing," *Ultrasonics* **13**, 251–261 (1975).
- ²⁶E. H. Trinh, "Compact acoustic levitation device for studies in fluid dynamics and material science in the laboratory and microgravity," *Rev. Sci. Instrum.* **56**, 2059–2065 (1985).
- ²⁷C. A. Rey, D. R. Merkley, G. R. Hammarlund, and T. J. Danley, "Acoustic levitation technique for containerless processing at high temperatures in space," *Metall. Trans. A* **19**, 2619–2623 (1988).
- ²⁸C. A. Rey, D. R. Merkley, S. Hampton, J. DeVos, D. Mapes-Riordan, and M. Zatarski, "Containerless processing at high temperatures using acoustic levitation," *Adv. Space Res.* **11**, 69–77 (1991).
- ²⁹J. K. R. Weber, D. S. Hampton, D. R. Merkley, C. A. Rey, M. M. Zatarski, and P. C. Nordine, "Aero-acoustic levitation: A method for containerless liquid-phase processing at high temperatures," *Rev. Sci. Instrum.* **65**, 456–465 (1994).
- ³⁰P. C. Nordine, D. Merkley, J. Sickel, S. Finkelman, R. Telle, A. Kaiser, and R. Prieler, "A levitation instrument for containerless study of molten materials," *Rev. Sci. Instrum.* **83**, 125107 (2012).
- ³¹A. Marzo, A. Barnes, and B. W. Drinkwater, "TinyLev: A multi-emitter single-axis acoustic levitator," *Rev. Sci. Instrum.* **88**, 085105 (2017).
- ³²V. Contreras and A. Marzo, "Adjusting single-axis acoustic levitators in real time using rainbow schlieren deflectometry," *Rev. Sci. Instrum.* **92**, 015107 (2021).
- ³³A. Marzo, T. Corkett, and B. W. Drinkwater, "Ultraino: An open phased-array system for narrowband airborne ultrasound transmission," *IEEE Trans. Ultrason., Ferroelectr., Freq. Control* **65**, 102–111 (2018).
- ³⁴A. N. Clark, C. E. Lesher, S. D. Jacobsen, and Y. Wang, "Anomalous density and elastic properties of basalt at high pressure: Reevaluating of the effect of melt fraction on seismic velocity in the earth's crust and upper mantle," *J. Geophys. Res.: Solid Earth* **121**, 4232, <https://doi.org/10.1002/2016jb012973> (2016).
- ³⁵S. M. Argyri, C. Andersson, N. Paillet, L. Evenäs, J. Ahrens, A. Marzo, V. Contreras, and R. Bordes, "Customized and high-performing acoustic levitators for contact-free experiments," *J. Sci.: Adv. Mater. Devices* **9**, 100720 (2024).
- ³⁶G. S. Settles, *Schlieren and Shadowgraph Techniques* (Springer, Berlin Heidelberg, 2001).